Macromolecules

pubs.acs.org/Macromolecules Article

High Molecular Weight Biobased Long-Chain Aliphatic Polyesters with Degradability: Insights into Mimicking Polyethylene

Nagarjuna A. Mahadas, Amir Suhail, Martin Taylor Sobczak, Xiaomeng Li, Kezhi Chen, Kenan Song, Guangbin Dong, Olga Kuksenok,* and Chuanbing Tang*

Cite This: *Macromolecules* 2025, 58, 4070–4081 Read Online

ACCESS | Metrics & More | Article Recommendations | Supporting Information

ABSTRACT: Synthesis of high molecular weight long-chain aliphatic polyesters with mechanical properties similar to polyethylene is challenging. This study presents high molecular weight biobased polyesters synthesized via a three-step process involving transesterification, polycondensation, and postcondensation, using biobased 1,18-dimethyl octadecanedioate (C_{18}-diester) and natural diols ranging from C_3 to C_{12}. All polyesters achieved weight-average molecular weights over 110 000 g/mol. The crystalline structures and thermomechanical properties of polyesters were largely influenced by the chain length of diols, with an odd−even effect observed. These polyesters exhibit tensile properties mimicking HDPE and LDPE, which allowed successful processing into filaments and 3D-printed objects. Although these polyesters exhibit semicrystalline structures similar to polyethylene, their melting temperatures are significantly lower, especially compared to HDPE. Chemical recycling of a representative polyester demonstrated its ability to undergo depolymerization and repolymerization, with the recovered polyesters displaying comparable mechanical properties to the virgin one. Coarse-grained molecular dynamic simulations of these polyesters demonstrated crystallization of the materials upon cooling from melts and reproduced the decrease in crystallization temperature with an increase in the ester-to-methylene ratio observed in the experiments. The proposed modeling approach allowed us to track the growth of crystalline domains upon cooling from the melt by characterizing the local nematic order parameter to quantify the effect of ester groups on the crystallization process. This study addresses common challenges that complicate synthesis and polymer processing, providing useful guidance for achieving reproducible polyester preparation.

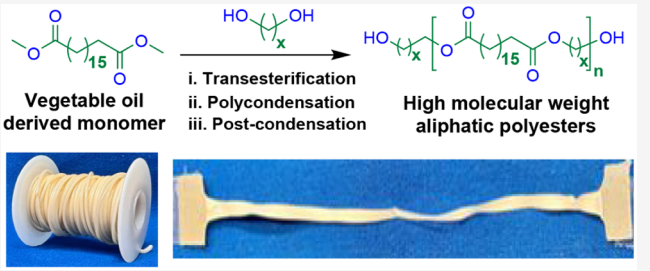

1. INTRODUCTION

Polyolefins are the most consumed plastics, accounting for over 50% of global plastic demand and reaching over 180 million tons in 2022.[1−3] Polyolefins, such as high-density polyethylene (HDPE) and low-density polyethylene (LDPE), are known for their durability, flexibility, and chemical stability. HDPE, with its highly linear chain structure, boasts excellent mechanical strength due to its high crystallinity. LDPE, with its branching, offers greater flexibility but relatively lower strength and crystallinity.[4] Despite their many benefits, polyolefins pose significant environmental challenges due to their chemically nondegradable nature and the negative consequences of undesirable breakdown into microplastics.[5,6]

Chemical recycling and upcycling of polyethylene have recently received much attention;[7−9] however, the development of energy-efficient and selective catalytic processes is hindered by the chemical inertness of the C−C and C−H bonds in polyethylene.[10] Therefore, transitioning from a linear to a circular economy is critical for reducing plastic waste and maximizing the value of plastic materials.[11] This involves the design of plastics with built-in mechanisms for degradation and recycling. One promising approach involves incorporating cleavable functional groups (e.g., ester, carbonate, amide, acetal) into polyolefins to enable chemical recycling, producing polymers that can be depolymerized and repolymerized.[12−24]

On the other hand, polyesters, including poly(lactic acid), polyhydroxybutyrate, poly(ϵ-caprolactone), and poly(butylene succinate), are widely used in industries such as packaging and medicine. However, their brittleness and limited elongation at break, restrict their use as polyethylene alternatives.[25,26] Long-chain aliphatic polyesters offer a promising alternative to traditional polyolefins. These materials possess cleavable functional esters that facilitate degradation under optimized conditions. The commercial availability of biobased aliphatic diesters, like C_{18}-diacid produced by Wilmar from palm oil via olefin metathesis, has advanced the field. Similar technologies could be applied to other fatty acid feedstocks.[27] These long-

Received: January 19, 2025
Revised: March 4, 2025
Accepted: March 27, 2025
Published: April 7, 2025

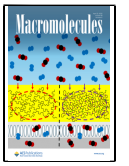

Scheme 1. Synthesis of Biobased Polyesters (PES-*x*, 18) Using C_{18}-Diester and Varying Diols (*x* Represents the Number of Carbons from a Diol)

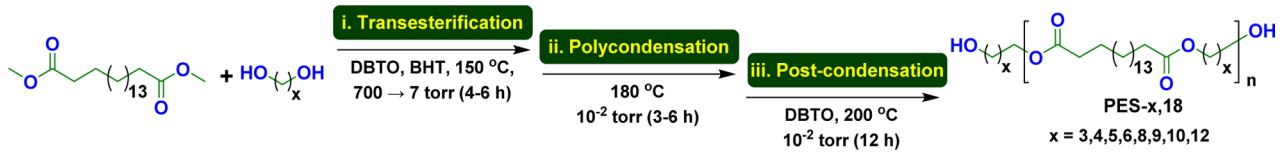

chain α,ω-difunctional compounds are of interest as monomers for polycondensates because the long methylene sequences impart crystallinity. As a result, long-chain aliphatic polyesters can have melting points that are high enough for thermoplastic processing.[28] Roumanet et al. synthesized polyesters with varying unsaturation levels in the polymer backbone based on 1,18-(*Z*)-octadec-9-enedioic acid and investigated thermal properties and degradability with the varying unsaturation content.[25]

Recent studies, particularly those conducted by the Mecking group, have developed long-chain aliphatic polyesters with mechanical properties similar to HDPE and LDPE. They synthesized fully recyclable polyesters from bioderived 1,18-dimethyl octadecanedioate (C_{18}-diester) and C_{18}-diol, achieving HDPE-like properties. These polymers demonstrated closed-loop recyclability through depolymerization and repolymerization.[29] The Mecking group also reported that polyesters synthesized from C_{18}-diester and 2,3-butanediol exhibited LDPE-like mechanical properties, marking a significant step toward developing viable, eco-friendly alternatives to conventional polyolefins.[30] Nature itself offers a wealth of linear short-chain diacids, from malonic acid to 1,12-dodecanedioic acid, which can be converted into their respective diols, such as 1,3-propanediol and 1,12-dodecanediol, to develop new polyesters.[29,31−33]

One of the major challenges in step-growth polymerization is the achievement of a high molecular weight, which is essential for mechanical and thermal properties. There are a variety of associated factors complicating the synthesis that are usually not reported in detail. This is particularly troublesome for achieving reproducibility within the scientific community. In this work, long-chain aliphatic polyesters were prepared from vegetable oil-derived C_{18}-diester with varied chain lengths of biobased linear aliphatic diols (carbon numbers 3, 4, 5, 6, 8, 9, 10, 12) (Scheme 1). The synthesis methodology, involving transesterification, polycondensation, and postcondensation, was detailed to increase the molecular weight of the polymers. Consequently, their tensile properties are comparable to or better than those of polyethylene. Different lengths of linear diols are worth exploring because of the odd−even carbon chain effect,[26,27,34] which, in linear aliphatic polyesters, refers to the periodic variation in thermal and mechanical properties based on the odd and even number of methylene units in the diol or diester segments, due to differences in molecular packing. Furthermore, depolymerization and repolymerization for a representative polyester were demonstrated to show the potential for closed-loop recycling. Coarse-grained molecular dynamic simulations of these polyesters captured the crystallization of these materials from melts upon cooling and melting of the crystalline regions upon heating. Our modeling results reproduced the decrease in crystallization temperature with an increase in the ester-to-methylene ratio, as observed in the experiments. It is worth mentioning that this method, using fatty acids as precursors, would have to overcome challenges to achieve melting temperatures comparable to those of HDPE and/or LDPE, which will also be discussed.

2. RESULTS AND DISCUSSION

2.1. Synthesis of Biobased Polyesters Using C_{18}-diester and Aliphatic Diols (C_3−C_{12}). The vacuum control and the prevention of cross-linking are two elements of advances from this study. This section aims to describe the reaction conditions and potential pitfalls in greater detail to ensure reproducibility of the work within the scientific community. Such specificity is essential given the complexities of polymer conditions and processes, which are often underreported. A series of reactions were performed on 1,18-diester with eight biobased diols (C_3, C_4, C_5, C_6, C_8, C_9, C_{10}, and C_{12}) to investigate the control of molecular weight and the impact of varying chain lengths on the thermomechanical properties of polyesters. Due to the unavailability of C_7 and C_{11} diols, their corresponding polyesters were not synthesized. In view of the diols used, all can be derived from biobased resources; thus, the biobased carbon content in synthesized polyesters could be 100%. Diester was chosen instead of diacid for better reaction yield, as diacid requires higher temperatures (220−240 °C) in polymerization, which would result in partial degradation of the diacid. To achieve high molecular weight, we discovered that it was necessary to employ three steps: sequential transesterification, polycondensation, and postcondensation. Dibutyltin oxide (DBTO) was used as a catalyst, as shown in Scheme 1. DBTO in solid granule form was opted for ease of performing the reaction instead of $Ti(O^nBu)_4$ which requires a solvent for the addition, though the efficiency of both catalysts is similar.[30,33] Furthermore, it has been reported that $Ti(O^nBu)_4$ can introduce monofunctional end groups, potentially limiting polymer molecular weight, whereas DBTO does not pose this limitation.[35] During the investigation on the synthesis of aliphatic polyesters, it was discovered that polymers could be cross-linked in the reaction system if radical inhibitors were absent or if an improper vacuum was applied. Thus, a radical inhibitor, such as butylated hydroxytoluene (BHT) was used. During the first step of transesterification of C_{18}-diester and diol, methanol was removed as a byproduct under continuous nitrogen purging. The reaction continued until 90% of the calculated amount of methanol was generated. The reaction was purged with nitrogen (typically for 2 h) until the reaction mixture was observed to be melted, indicating oligomerization had commenced, followed by polycondensation of the oligomers under a regulated vacuum. All reactions with different diols were carried out under similar processes. However, the vacuum was controlled based on the volatility of a specific diol.[26] The stoichiometric quantities of diols from C_3 to C_{10} were used in two equivalents, while diol C_{12}, being less volatile, required strictly one equivalent. Initially, for diols from C_3 to C_8 and from C_9 to C_{12}, the reaction temperature was 150 and 180 °C,

https://doi.org/10.1021/acs.macromol.5c00176
Macromolecules 2025, 58, 4070−4081

respectively. Transesterification was followed by polycondensation at 7 Torr until a viscous mixture formed, as determined by the stirring speed of the stir bar. A gradually decreasing and regulated vacuum was mandatory to prevent premature loss of diol from the reaction.[30] The temperature was then increased to 180 °C to facilitate further polymerization. At the same time, a high vacuum (10^{-2} Torr) was used to remove the residual diol, preventing reversible reactions that could result in low molecular weight polyesters.[34] Both temperature and vacuum control were meticulous but highly necessary for achieving high molecular weight.

After polycondensation, the synthesized polyesters could have a number-average molecular weight (M_n) as high as >20 000 g/mol, characterized by high-temperature gel permeation chromatography (HT-GPC); however, many of these polymers are still brittle or do not reveal better properties. The molecular weight of these polymers was further increased by employing a strategy called postcondensation, as these polyesters consist of −OH groups on one or both ends of the polymer, which could allow further polymerization. Therefore, the obtained polymers were postpolymerized with the addition of a catalyst at 200 °C with continuous stirring. The molecular weights obtained from consecutive polycondensation and postcondensation of polymers generally increased by more than 50% (Table 1). All weight-average molecular weights (M_w) consistently exceed 110 000 g/mol.

Table 1. Molecular Weight Information for PES-*x*,18, Determined Using NMR and HT-GPC

	Polycondensation	Postcondensation			
	(HT-GPC)	HT-GPC			NMR
Sample	M_n (g mol^{-1})	M_n (g mol^{-1})	M_w (g mol^{-1})	$Đ$	M_n (g mol^{-1})
PES-3,18	13 100	53 300	137 600	2.6	33 700
PES-4,18	34 200	48 900	139 300	2.8	49 100
PES-5,18	29 800	46 500	130 400	2.8	34 100
PES-6,18	20 300	43 700	127 200	2.9	31 300
PES-8,18	34 300	42 100	112 800	2.7	32 300
PES-9,18	31 500	58 400	233 100	4.0	18 400
PES-10,18	5300	54 500	231 400	4.3	37 200
PES-12,18	42 900	66 700	189 200	2.8	100 100

The ^{1}H NMR spectra of this series of polyesters are shown in Figures 1 and S2−S9. For each polymer, the triplet peak around 3.66 ppm is attributed to the methylene protons from $HOCH_2-$ at both terminals, except for PES-12,18, as it has one terminal as a methyl ester $-OCH_3$, which displays as a singlet peak. The characteristic peaks of the methylene protons ($O{=}C{-}CH_2$) adjacent to the carbonyl group in all polymers have a chemical shift around 2.3 ppm. For all polyesters, the resonance peaks near 1.50−1.70 ppm and 1.20−1.40 ppm correspond to the protons of the internal methylene groups in the polymer backbone. The M_n of the polymers in Table 1 is determined using the ester protons $-COOCH_2$ at the chemical shift of 4.10−4.30 ppm and their integration ratio to the terminal $HOCH_2-$. ^{1}H NMR revealed the successful synthesis of high molecular weight polyesters with the expected chemical structure. In comparison, HT-GPC analysis revealed the M_n of these biobased polyesters to be in the range of ∼40 000 g mol^{-1} to ∼70 000 g mol^{-1} and M_w over 110 000 g/mol when using polystyrene standards (Table 1). GPC traces of the polymers are included in Figures S10−S17.

2.2. Thermal Properties of Polyesters. Thermal transitions of polyesters were examined by using differential scanning calorimetry (DSC). The DSC thermograms are included in Figures S18−S25 and the thermal transitions are tabulated in Table 2. The influence of the carbon chain length on the melting temperature (T_m) and enthalpy of crystallization (ΔH_c) is plotted in Figure 2a. All polymers exhibit melting temperatures and enthalpy of crystallization ranging from 81 to 93 °C and 68 to 143 J/g, respectively. Moreover, during the cooling process, all biobased polyesters exhibited single crystallization peaks with varying enthalpies depending on the chain lengths of the diols. This single crystallization peak indicates the semicrystalline nature of the polymers, similar to polyethylene. Among all polyesters, PES-12,18 revealed the maximum thermal transition properties owing to its long aliphatic chain and even number of carbons between the ester functionalities, providing a better arrangement of polar functionalities in the polymer.[30] The melting and crystallization temperatures of polymers with an odd number of carbons (PES-3,18, PES-5,18, and PES-9,18) are lower than those with the corresponding even number of carbons (PES-4,18, PES-6,18, and PES-8,18). The melting transitions of all polymers revealed an overall zigzag-rising trend attributed to the mismatching of ester functionalities in the polymers, as shown in Figure 2.[27,36] These odd−even effects observed in this study are similar to and most pronounced for short distances between ester groups, which corroborates those reported in the literature.[26,34,36,37]

Melting temperatures of these polyesters in this work are significantly lower compared to commercial LDPE (T_m = 105−115 °C) and HDPE (T_m = 120−135 °C) due to the high density of ester functionalities relative to methylene groups in the crystal lattice, creating an energy penalty and reducing the crystal packing energy.[38] It is worth noting that most polyethylene mimics derived from biobased fatty acids are unlikely to match the melting temperature of commercial polyethylene unless extremely long fatty derivatives (e.g., C48) are used.[39] However, producing such long-chain derivatives remains economically impractical with current technologies. Polyethylene mimics prepared by ring-opening metathesis polymerization, as reported in the literature[18,38] and by us,[40] show comparable melting temperatures to commercial polyethylene. However, this method is unlikely to be scalable; nevertheless, it could provide useful insights into structure−property relationships.

2.3. Wide Angle X-Ray Diffraction (WAXD). WAXD deconvolution analysis was conducted to examine the crystalline structure and degrees of crystallinity (χ) of polyesters, as summarized in Table 2 and Figures S26−S33. Stacked scattering profiles of polyesters in Figure 3 indicate that all polyesters exhibited similar peak shapes and positions at 2θ = 21.6°, 24.1°, and 30.0°. These peaks correspond to the [110], [200], and [210] planes, respectively, consistent with the orthorhombic solid-state structure typical of HDPE and LDPE.[29,33,41,42] The degree of crystallinity is low at 35.5% for PES-3,18. It increases to 45.5% for PES-4,18, and the value almost remains constant at 52.3 ± 0.1% from PES-5,18 to PES-8,18, and increases to 54.6% for PES-12,18. The long aliphatic C_{18}-diester imposed a higher crystalline structure in PES-3,18, which was absent in previously reported polyesters based on C_{12}-diacid or C_3.[26] For polyesters derived from longer-chain

https://doi.org/10.1021/acs.macromol.5c00176
Macromolecules 2025, 58, 4070−4081

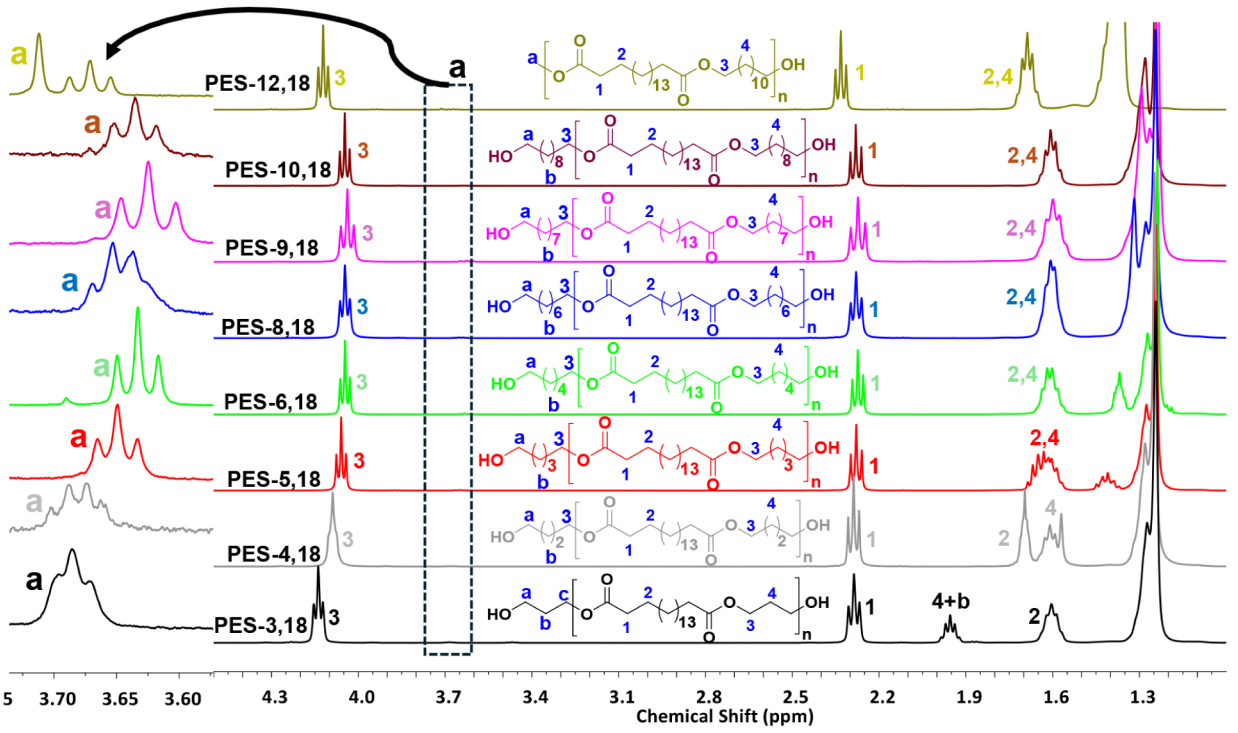

Figure 1. Stacked ^{1}H NMR spectra of biobased polyesters: the inset indicates the end group.

Table 2. Thermal Transitions and Degree of Crystallinity of Aliphatic Polyesters

	Thermal transitions					
Sample	T_m (°C)	T_c (°C)	ΔH_m (J/g)	ΔH_c (J/g)	$\chi_{c,dsc}$ (%)[b]	χ (%)[a]
PES-3,18	81	61	48	68	16.7	35.5
PES-4,18	87	73	110	98	38.2	45.5
PES-5,18	82	67	114	107	39.6	52.2
PES-6,18	89	72	107	123	37.2	52.4
PES-8,18	90	71	127	131	44.1	52.4
PES-9,18	86	68	112	110	38.9	59.1
PES-10,18	90	75	117	137	40.6	54.6
PES-12,18	93	76	143	140	49.7	54.6
LDPE	109	98	62	75.3	21.5	39.1
HDPE	127	114	174	194	60.4	58.9

[a]Degree of crystallinity determined using the deconvolution of WAXD data. [b]$\chi_{c,dsc}$ was calculated from melting enthalpies obtained from DSC using the formula mentioned in the Characterization section.

C_{18}-diesters, the ester bond content is relatively lower, enabling their chain structures to more closely resemble those of polyethylene. Consequently, their crystalline structures are similar to polyethylene.

2.4. Mechanical Properties. The mechanical properties of these polyesters are key indicators of their strength and toughness. Tensile testing of low molecular weight polyesters obtained after polycondensation was first performed. Tensile properties, such as tensile strength, elongation at break, and modulus, are strongly influenced by the polymer's molecular weight. Polymers with a lower molecular weight have fewer entanglements, leading to weaker intermolecular interactions and lower tensile strength, elongation at break, and modulus.[43] Figure S43a,b of these lower molecular weight polyesters clearly indicates lower tensile properties. Images of a few of the polyesters are shown in Figure S43c. The heterogeneity indicated a poor quality in the films.

Tensile testing of polyesters obtained after postcondensation was then performed. The stress−strain data are summarized in Table 3, and representative stress−strain curves are shown in Figures 4 and S34−S41. All data represent the average values based on measurements in triplicate. Digital images of the molded dog-bone specimens before and after tensile testing are shown in Figures S34b,c−S41b,c. These polyesters exhibited Young's modulus in the range of E_t = 120−501 MPa, a yield strength of σ_y = 11.7−18.5 MPa, and an elongation at break of ε_{tb} = 431−670%. It appears that polyesters from even diols (PES-12,18) resemble HDPE better, while odd diols result in polymers in the range of LDPE.

An even number of carbon-containing diols led to polyesters with a higher tensile modulus compared to an odd number of carbon-containing diols. Young's modulus, yield stress, tensile stress at break, and elongation at break increase as the length of the carbon chain increases in even- or odd-diol-based polyesters, respectively. PES-12,18 revealed the highest tensile stress, comparable to commercial HDPE. This is attributed to the even and higher carbon chain length. Overall, the tensile properties demonstrate the versatility of C_{18}-diester-based polyesters, providing tunable mechanical properties ranging from HDPE-like to LDPE-like behavior by adjusting the chain length of the diols (Figure 4c).

It is worth mentioning that sample processing could have a substantial effect on the mechanical properties. We found that after hot pressing, the specimen should rest at ambient temperature for at least 24 h to achieve optimal tensile properties. Tensile properties immediately after hot pressing (within 30 min) resulted in low mechanical performance (Figure S42).

2.5. 3D Printing of the Biobased Polyester. The thermal and tensile properties of the synthesized polyesters

https://doi.org/10.1021/acs.macromol.5c00176
Macromolecules 2025, 58, 4070−4081

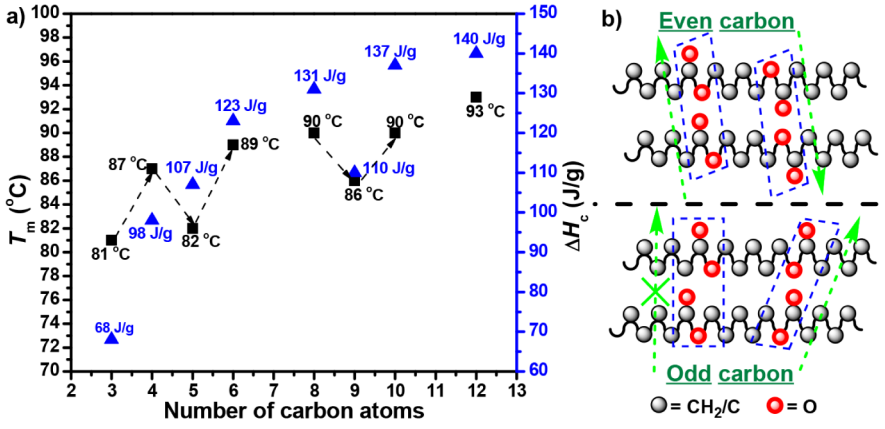

Figure 2. (a) Melting temperature (T_m) and enthalpy of crystallization (ΔH_c) of PES-*x*,18 as a function of the number of carbon atoms in the diols; (b) schematic illustration of the arrangements of the polar layers with even and odd effects accounting for the melting behavior.

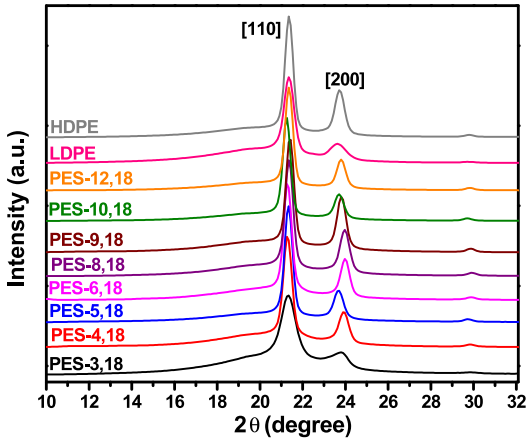

Figure 3. WAXD profiles of biobased polyesters PES-*x*,18.

Table 3. Tensile Properties of Biobased Polyesters PES-*x*,18

	Tensile properties			
Sample	Young's Modulus E_t (MPa)	Yield Stress σ_y (MPa)	Tensile stress at break σ_b (MPa)	Elongation at break ε_b (%)
PES-3,18	120 ± 6	12.2 ± 1	15.3 ± 1.4	439 ± 83
PES-4,18	336 ± 19	14.3 ± 0.4	16.6 ± 0.5	431 ± 4
PES-5,18	224 ± 28	11.9 ± 0.4	12.8 ± 3.1	502 ± 153
PES-6,18	415 ± 56	15.8 ± 0.9	15.9 ± 3.3	591 ± 117
PES-8,18	381 ± 4	15.9 ± 0.3	15.1 ± 1.3	595 ± 74
PES-9,18	257 ± 10	11.7 ± 0.3	12.9 ± 1.7	686 ± 71
PES-10,18	392 ± 1	15.8 ± 0.8	12.9 ± 2.3	419 ± 139
PES-12,18	469 ± 33	17 ± 1.9	14.5 ± 1.5	559 ± 104
LDPE	104 ± 34	8.8 ± 0.3	8.3 ± 0.4	187 ± 81.3
HDPE	367 ± 19	18 ± 0.9	8.7 ± 1.1	148 ± 104

exhibit relatively low melting temperatures (T_m) and crystallization temperatures, along with favorable mechanical properties, which make them ideal for melt processing techniques. To explore their processability, we selected PES-5,18 (a mimic of LDPE) as a case study and evaluated its behavior in 3D printing. PES-5,18 was successfully 3D printed using fused deposition modeling (FDM) on a Hyrel Hydra 21 platform. The filament for FDM was extruded using an Xplore MC-5 microcompounder (Figure 5a). The 3D printer nozzle temperature was set at 120 °C, and the bed temperature was set at 73 °C to control the cooling rate near the crystallization temperature, thereby inhibiting warping and increasing bed adhesion, which is an inherent problem when working with any molecular weight of PE.[44,45] Variations in bed temperatures from 30 to 80 °C were tested, but the best results were derived at 73 °C. Figure 5b,c illustrates the 3D printing process and a printed logo, showcasing the potential applications of biobased, linear, long aliphatic chain polyesters in cutting-edge technologies.

2.6. Recycling of the Biobased Polyester. Solvolysis reactions in the depolymerization of polyesters for chemical recycling, such as poly(ethylene terephthalate), are well-known.[46] Recently, the degradation of PES-2,18 and PES-18,18 was also performed in methanol with closed-loop recycling of these polymers.[29,33] In this work, high molecular weight PES-12,18, as a representative polyester, was subjected to depolymerization in methanol. A dimer (~2 repeat units) was recovered, as shown in ^{1}H NMR spectra (Figure S44), instead of a mixture of C_{18}-diester and C_{12}-diol from the polymer. HT-GPC analysis also revealed complete depolymerization of the polymer to the dimer (M.W. = 950 g mol^{-1}), as shown in Figure S45. The recovered dimer was further used for a polycondensation reaction with the addition of the catalyst DBT. HT-GPC analysis of the polycondensation and postcondensation-prepared polyesters revealed M_n as 25 100 g mol^{-1} and 46 300 g mol^{-1}, respectively. The molecular weight of repolymerized PES-12,18 is comparatively lower with respect to the virgin polymer, possibly due to the stoichiometric imbalance of the monomers after depolymerization and workup.

Tensile testing was performed on recycled PES-12,18 and compared with that of virgin PES-12,18 (Figure 6). The tensile properties of recycled PES-12,18 revealed comparable yield stress [σ_y (average) = 17.2 MPa] and lower elongation at break [ε_b (average) = 335%] compared to the virgin PES-12,18. This may be attributed to the relatively lower molecular weight obtained during repolymerization compared to the virgin PES-12,18.

2.7. Computational Modeling Studies. The common challenges that complicate polymer synthesis and processing

https://doi.org/10.1021/acs.macromol.5c00176
Macromolecules 2025, 58, 4070−4081

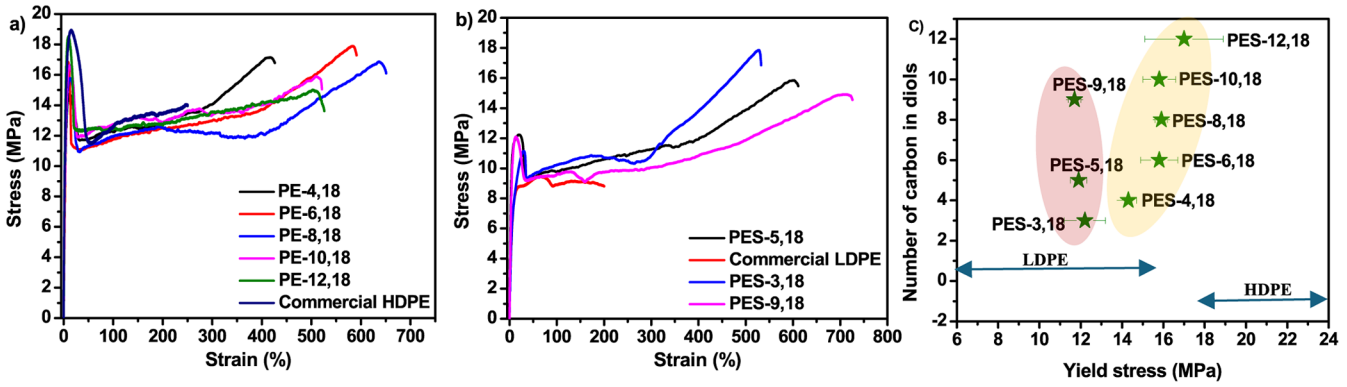

Figure 4. Stress–strain curves of hot-pressed and dog-bone molded biobased aliphatic polyesters PES-*x*,18: a) even number of carbons in diol and commercial HDPE; b) odd number of carbons in diol and commercial LDPE; c) effect of the odd–even chain length of the diols resulting in tensile properties (yield stress) in the range of LDPE and HDPE.

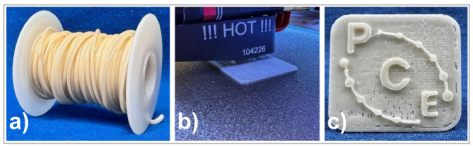

Figure 5. (a) Extruded filament of PES-5,18 using Xplore MC-5 microcompounder; (b) 3D printing process of the object; (c) 3D-printed logo of Center for Polymer for a Circular Economy (PCE).

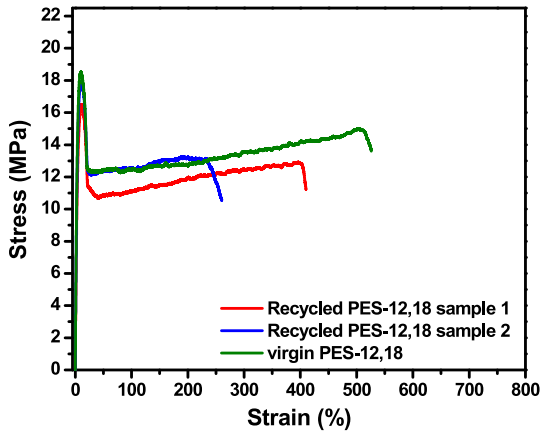

Figure 6. Stress–strain curves of hot-pressed samples of virgin and repolymerized PES-12,18.

can be guided by computational modeling to achieve reproducibility. We used coarse-grained molecular dynamics simulations to capture the cooling and heating processes for polyesters listed in Table S1 and compare these processes with the cooling and heating of pure polyethylene (PE). The schematic diagram of a polyester chain considered in our simulations is provided in Figure 7a, where PE and ester beads are colored blue and red, respectively. We adapted the united monomer (UM) model,[47−49] which accurately captures crystallization in polyethylene.[47,49−54] Within this model, a single PE bead represents two carbon atoms. Hence, to model polyester chains closely matching the systems considered in experiments, we alternate 8 PE beads (16 carbon atoms) and $\bar{x}$ PE beads ($2\bar{x}$ carbon atoms) between ester groups, as shown in the schematic diagram of Figure 7a. In our simulations, we choose $\bar{x}$ between 2 and 6, so that the systems considered are PES-4,18, PES-6,18, PES-8,18, PES-10,18, and PES-12,18, respectively, along with pure PE (see Table S1). A single bead represents the ester group.[40] For the PE beads, we used the force field developed by Fall et al.[47] The nonbonded interactions between the beads separated by a distance below the cutoff radius $r_c = 1.02\sigma$, where σ is the size of the bead, are captured by the Lennard-Jones (LJ) potential as $U_{LJ} = 4\varepsilon\left[\left(\frac{\sigma}{r}\right)^9 - \left(\frac{\sigma}{r}\right)^6\right]$, where ε is the strength of the potential. The parameters describing LJ interactions between the ester beads[40] are set with respect to the parameters describing LJ interactions between the PE beads[47] as follows: the size of the ester bead, σ_E with respect to that of the PE bead, σ, is set at $\sigma_E = 0.77\sigma$, based on the empirical density relation for organic materials,[55] and the mixing rule $\sigma_{E-PE} = (\sigma_E\sigma)^{1/2}$ is used for the interactions between ester and polyethylene beads. The strengths of the LJ interaction between the ester beads, ε_E, and between the ester and PE beads, ε_{E-PE}, with respect to the strength of the LJ interaction between the PE beads, ε, are chosen based on the interaction parameters in the Martini force field.[56] Specifically, we set $\varepsilon_E = 1.14\varepsilon$ and $\varepsilon_{E-PE} = 0.77\varepsilon$, where ε is given by the force field[47] for PE, and the values of $\varepsilon_E/\varepsilon$ and $\varepsilon_{E-PE}/\varepsilon$ are chosen[40] based on the ratios of $\varepsilon_{N_a-N_a}/\varepsilon_{C_2-C_2}$ and $\varepsilon_{N_a-C_2}/\varepsilon_{C_2-C_2}$ in the Martini force field,[56] respectively, where N_a and C_2 are bead types in the Martini force field. The angular potential and the bond length are kept the same for all of the beads. Simulations were performed using the LAMMPS open-source simulation package,[57,58] and visual molecular dynamics (VMD) software[59] was used to generate simulation snapshots and calculate the local order parameter as defined below. In all of the simulations, 384 linear chains with 200 beads in each chain were considered. The initial chain distribution was generated using dissipative particle dynamics[60] simulations, and the equilibration was performed as detailed in ref 47.

We first equilibrated a melt of PE chains for 3.7×10^8 time steps with periodic boundary conditions, then replaced some of the PE beads with ester beads, as shown schematically in Figure 7a and equilibrated the system with ester beads for an additional 1.5×10^8 time steps. The equilibrated melts were first subjected to cooling from 500 to 250 K at a rate of 0.1 K/ns, and then the same systems were subjected to heating from 250 K to 500 K at the same rate of 0.1 K/ns. A Nose-Hoover thermostat and barostat, with damping parameters chosen as[47] 2 τ and 100 τ, respectively, and an integration time step of

https://doi.org/10.1021/acs.macromol.5c00176
Macromolecules 2025, 58, 4070−4081

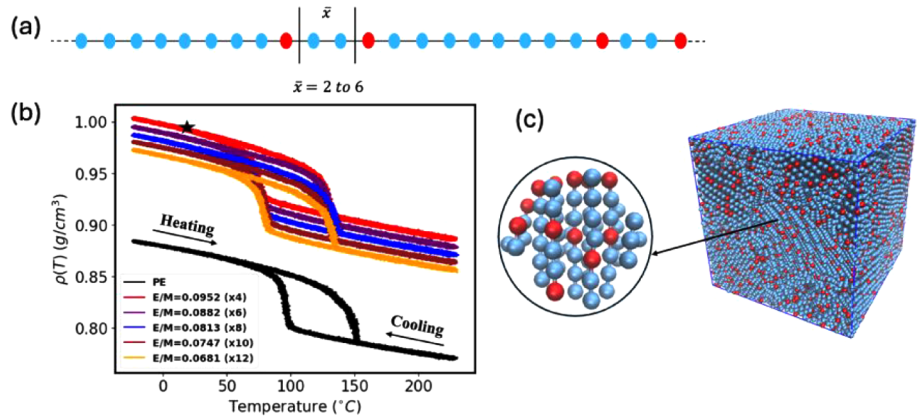

Figure 7. (a) Schematic diagram of a polyester chain used in the simulations. The chain contains 200 beads, 8 PE beads and $\bar{x} = 2$ PE beads are alternated between the ester groups (in red). (b) Density−temperature profile of pure PE (in black) and polyesters with various values of $\bar{x}$ and respectively, various ester-to-methylene (E/M) ratios as provided in the legend. Arrows indicate directions of density change during cooling (right-to-left) and during heating (left-to-right); (c) Simulation snapshot of a semicrystalline polyester with $\bar{x} = 2$ upon cooling to $T = 20$ °C, the inset shows morphology within the selected crystalline region.

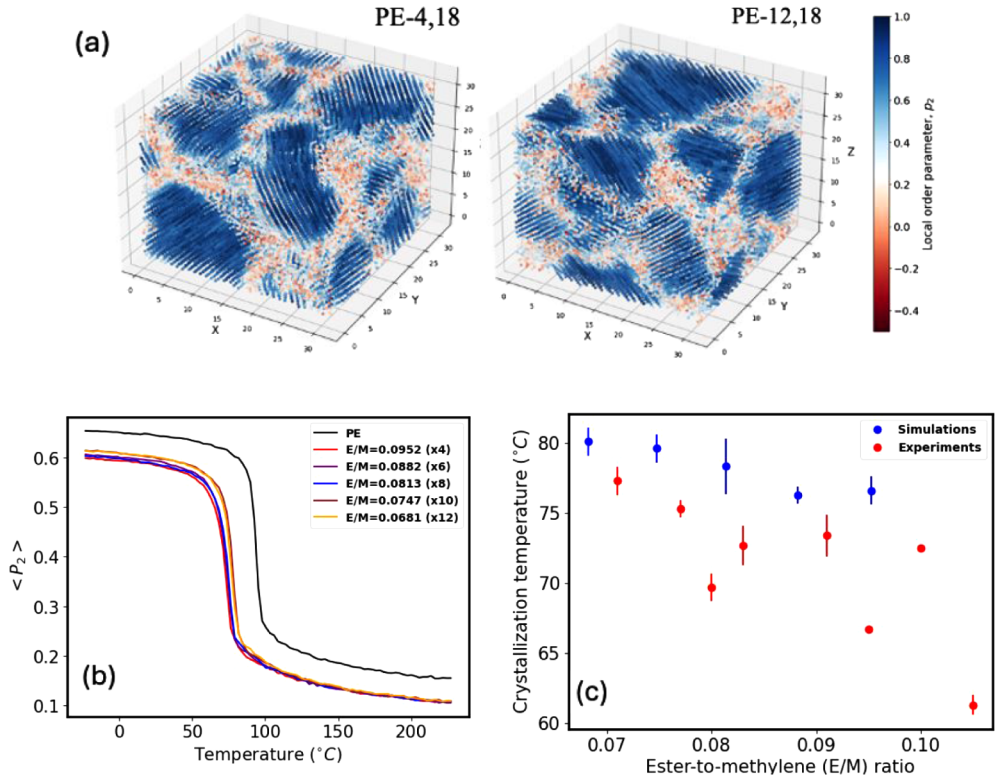

Figure 8. (a) The distribution of the local order parameter p_2 in the semicrystalline phases at $T = 20$ °C for polyesters with $\bar{x} = 2$ (left image) and $\bar{x} = 6$ (right image). p_2 is shown for each bead according to the scale bar on the right with ordered crystalline regions shown in dark blue. (b) Average local order parameter, $< P_2 >$, calculated during cooling processes for pure PE (in black) and polyesters with various values of $\bar{x}$ and correspondingly various ester-to-methylene (E/M) ratios as provided in legend. (c) Crystallization temperature as a function of ester-to-methylene (E/M) ratio; blue circles correspond to the simulation results, and red circles correspond to the experimental data points.

0.005 τ (which corresponds to 2.7 ps) were used to model the crystallization and melting processes.

The densities of all systems during cooling and heating for pure PE (in black) and for a range of polyesters, as marked in the legend, are shown in Figure 7b. The bottom branch of each curve, from right to left, corresponds to the cooling process. A clear increase in density is observed for all of the cases upon cooling, with an abrupt jump in density at a critical temperature corresponding to the crystallization temperature. The simulation snapshot of the sample morphology for PES-4,18 at $T = 20$ °C is shown in Figure 7c, with a close-up of a portion of the crystalline region shown in the inset. The star symbol in Figure 7b corresponds to the snapshot shown in Figure 7c.

The top branch of each curve in Figure 7b from left to right corresponds to the heating process, with an abrupt decrease in density corresponding to the melting temperature. An increase in the density of polyesters with respect to pure PE at all

https://doi.org/10.1021/acs.macromol.5c00176
Macromolecules 2025, 58, 4070−4081

temperatures, as well as a distinct shift of transition regions toward lower temperature values for all the polyesters compared to those for pure PE, as seen in Figure 7b, is consistent with recent findings in atomistic simulations of polyethylene functionalized with esters.[61]

The local nematic order parameter $p_2(i)$, which characterizes the bond ordering in the vicinity of each bead i, is often used to effectively quantify the degree of crystallinity in semicrystalline materials.[47,62−64] We calculate this value as $p_2(i) = \left\langle \frac{3\cos^2\theta_{ij} - 1}{2} \right\rangle_j$, where θ_{ij} is the angle between the vectors from $i - 1$ bead to $i + 1$ bead and from $j - 1$ bead to $j + 1$ bead, with the averaging taken over all the neighbors of bead i within the cutoff distance of 1.6σ.[47] In Figure 8a, we plot the local order parameter for each bead at a temperature of 20 °C for two polyesters (PES-4,18 and PES-12,18). The crystalline regions are shown in blue (high values of p_2) and the amorphous regions are shown in orange (low values of p_2) according to the scale bar on the right. We then characterize the average local order parameter of each system as a function of temperature (Figure 8b) as $< P_2 > = < p_2(i) >$, where the averaging is taken over all the beads in the simulation box during the cooling process. Sufficiently high values of $< P_2 >$ for the entire system correspond to the existence of crystalline domains. These plots show that there is a clear decrease in the average local order parameter $< P_2 >$ for all the polyester samples with respect to pure PE (in black); however, the differences between the considered examples incorporating ester groups (all remaining curves on the same plot) are negligibly small.

Finally, we calculate the crystallization (T_c) and melting (T_m) temperatures by first fitting the transition region of the enthalpy-temperature curve with a sigmoid function with four fitting parameters, and then finding the temperatures corresponding to the peaks in the derivative of this function, as detailed in our recent work.[40] Similar approaches were used in prior studies.[62,65] The crystallization temperatures calculated from our simulations for all of the polyester cases as a function of the ester-to-methylene (E/M) ratio are shown by the blue circles. In each case, the average values are calculated by using five independent simulations with different initial trajectories. The corresponding experimental values are shown as red symbols. These results indicate a decrease in T_c with an increase in E/M. We note that the decrease in T_c for all the polyesters with respect to pure PE is significantly more pronounced (compare temperatures corresponding to the abrupt changes during cooling in Figures 7b and 8b for pure PE and all the remaining curves, respectively). Finally, we also calculate melting temperatures and plot our simulation data as a function of the E/M ratio (Figure S46). These results show a pronounced decrease in melting temperature for all the polyesters with respect to that for pure PE; however, the differences between the temperatures for the polyesters considered within the relatively narrow range of E/M values in this work are small. The value of T_m for pure PE in Figure S46 is notably higher than that in experiments, which is consistent with prior studies reporting high values of T_m in coarse-grained simulations of polyethylene.[47,62] To summarize, our simulation results show the same trends for T_c and T_m as observed in our concurrent experiments.

3. CONCLUSIONS

In summary, biobased long-chain aliphatic polyesters using 1,18-dimethyl octadecanedioate and diols (C_3 to C_{12}) were successfully prepared through a three-step process of transesterification, polycondensation, and postcondensation. This study provides valuable insights into critical reaction conditions and processes to enhance the polymer molecular weight. The polyesters exhibited high molecular weights (M_w > 110 000 g/mol). Their thermal and mechanical properties varied with diol chain length. The crystallization and melting temperatures were higher for even−even polyesters compared to odd−even variants. Coarse-grained molecular dynamics simulations captured the crystallization upon cooling and melting upon heating in a range of polyesters and reproduced the decrease in crystallization temperature upon an increase in the ester-to-methylene ratio. Characterizing local nematic order parameters in simulations allowed us to track the growth of the crystalline domains upon cooling. Simulation results showed that the average order parameter, which effectively characterizes crystallinity within this system, remains high in the cooled state for all the polyesters considered. WAXD analysis of these polyesters revealed varying crystallinity, with the degree of crystallinity close to that of HDPE for the PES-9,18; PES-10,18; and PES-12,18 samples. With mechanical properties comparable to or better than polyethylene, these polyesters were able to be extruded into filaments for 3D printing into design objects. The potential of closed-loop recycling was demonstrated with a representative polyester. Though most long-chain aliphatic polyesters using biobased fats as monomers possess lower melting temperatures than commodity polyethylene, especially HDPE, these polyesters with robust mechanical properties could find useful applications in diverse industry sectors that traditional polyethylene cannot.

4. EXPERIMENTAL SECTION

4.1. Materials. 1,18-Dimethyl octadecanedioate (C_{18}-diester, 96%), 1,3-propanediol (PrD = 99.65%), 1,8-octanediol (OD, 99.92%), and 1,10-decanediol (DD, 97%) were procured from AmBeed Inc. 1,5-Pentanediol (PD, 98%), dibutyltin oxide (DBTO, 98%), 1,1,2,2-tetrachloroethane-[D_2] (TCE-d_2, 99.5% D) were purchased from Thermo Scientific. 1,6-Hexanediol (HD, >97%), 1,9-nonanediol (ND, >98%), 1,12-dodecanediol (DDD, >99%), and butylhydroxytoluene (BHT, ≥99%) were procured from TCI Chemicals. 1,4-Butanediol (BD, 99%) was purchased from Alfa Aesar. Chloroform-*d* was purchased from Cambridge Isotope Laboratories. 1,2,4-Trichlorobenzene (TCB) was purchased from Fisher Scientific. Xylene (mixture of isomers) was procured from StatLab. HDPE (lot no.: 08204BDV) and LDPE (lot no.: J16R014) were procured from Sigma-Aldrich and Alfa Aesar, respectively.

4.2. Synthesis of Biobased Polyesters. *4.2.1. Polycondensation.* For the typical synthesis of polyesters PES-*x*,18 (*x* is the number of carbons in the diol), a 50 mL Schlenk tube equipped with a stir bar was first dried under vacuum at 80 °C to remove moisture. For PES-3,18 to PES-8,18, the C_{18}-diester (3 g, 1 equiv), diol (2 equiv), and BHT (0.2 mol % w.r.t diol) were dried under vacuum at 80 °C in the tube. A condenser was attached to monitor the volatiles. After the addition of DBTO (0.5 mol %), nitrogen was purged through the mixture while ramping the temperature to 150 °C with stirring at 500 rpm. The reaction continued until volatiles ceased, followed by

https://doi.org/10.1021/acs.macromol.5c00176
Macromolecules 2025, 58, 4070−4081

gradual vacuum reduction from 700 to 7 Torr. Polycondensation proceeded at 150 °C for 16 h at 7 Torr, then the vacuum was reduced to 10^{-2} Torr and maintained at 180 °C for 3−6 h while stirring at 50 rpm. After cooling to 50 °C, the polymer was dissolved in dichloromethane and precipitated in methanol at −5 °C. The obtained polymer was filtered and dried under vacuum for 12 h at room temperature. A similar protocol of synthesis was followed for PES-9,18 and PES-10,18, except the polycondensation reaction temperature was set at 180 °C. For PES-12,18, DDD (1 equiv), C_{18}-diester (3 g, 1 equiv), and BHT (0.2 mol % w.r.t diol) were dried similarly, with nitrogen purged for 1 h post-DBTO addition, then heated to 180 °C (350 rpm). Vacuum was gradually reduced from 700 to 7 Torr over 6 h, followed by polycondensation at 180 °C for 16 h. After cooling, the polymer was dissolved in xylene and precipitated in isopropanol at −30 °C. The obtained polymer was filtered and dried under vacuum for 12 h at 50 °C. The resulting polyesters were designated as PES-x,18, where "18" is the carbon length of 1,18-dimethyl octadecanedioate and "*x*" represents the carbon length of the diol, e.g., a polyester from C_3 diol is termed PES-3,18.

4.2.2. Postcondensation. The polymer obtained from polycondensation was taken with the addition of DBTO (0.5 mol %) in a Schlenk tube equipped with a stirrer bar. The reaction was performed under high vacuum (~10^{-2} Torr) overnight at 200 °C. After the reaction was completed, the mixture was worked up as per the procedure given in polycondensation, resulting in a yield of 80−85%.

4.2.3. Synthesis of PES-5,18. C_{18}-diester (20 g, 1 equiv), diol PD (2 equiv), BHT (0.2 mol %, w.r.t diol), and DBTO (0.5 mol %) were added to the reaction flask, followed by a procedure similar to that mentioned above.

4.2.4. Chemical Depolymerization Experiment. PES-12,18 (3 g) and methanol (50 mL) were mixed in a thick-walled glass pressure vessel and sealed with a Teflon cap. The pressure vessel containing the polymer and solvent was placed in an oil bath at 120 °C for 24 h. Upon completion of the reaction, a precipitate formed, which was filtered and dried under vacuum overnight. The obtained solid was reprecipitated, filtered, and dried to obtain a white powder with a yield of 90%.

4.2.5. Repolymerization. The mixture of C_{18}-diester and DDD obtained postdepolymerization was repolymerized using the polycondensation and postcondensation conditions mentioned above.

4.3. Characterization. *4.3.1. Fourier Transform Infrared (FTIR).* FTIR spectra of polyesters and polyethylene were acquired by using a PerkinElmer Spectrum 100 FTIR spectrometer equipped with an attenuated total reflection (ATR) accessory. The absorption spectra were recorded at a resolution of 4 cm^{-1}, with signals averaged over 32 scans to enhance accuracy.

4.3.2. ^{1}H NMR Spectroscopy. ^{1}H spectra were recorded at 400 MHz on a Bruker Avance III spectrometer, using deuterated solvents such as chloroform-*d* ($CDCl_3$) and TCE-d_2. Chemical shifts (δ) are reported in parts per million (ppm), with tetramethylsilane (TMS) as the internal standard in $CDCl_3$ as the deuterated solvent.

4.3.3. High Temperature Gel Permeation Chromatography (HT-GPC). Molecular weights of the biobased polyesters were determined using high-temperature gel permeation chromatography in 1,2,4-trichlorobenzene (TCB) at 135 °C on a Tosoh Bioscience EcoSEC High Temperature GPC System (HLC-8321GPC/HT) with a dual-flow refractive index detector (HT-GPC instrument) equipped with PS-DVB columns [TSKgel GMHHR-H (S) HT2, 13 μm, 7.8 mm ID × 30 cm × 2, mixed bed] and an additional guard column. The flow rate of TCB was set to 1.0 mL min^{-1}. The GPC system was calibrated with polystyrene (PS) from PSS Laboratories. Molecular weights were determined via conventional calibration versus narrow polystyrene standards from PSS Polymer Standards (software: SECview, version 2.0).

4.3.4. Differential Scanning Calorimetry (DSC). Thermal properties of polymers were analyzed by using a HITACHI 7020 differential scanning calorimeter. A sample weighing 5−10 mg was placed in a 40 μL aluminum pan for measurement. Thermal analysis was performed in two stages: first, the sample was heated from 25 to 120 °C, followed by cooling back to 25 °C. In the second stage, the sample was heated to 200 °C to obtain melting data, followed by cooling back to 25 °C to capture crystallization data. Both heating and cooling were performed at a rate of 10 °C/min under a nitrogen atmosphere. The crystallinity ($\chi_{c,dsc}$) was calculated using eq 1:[66]

$$\chi_{c,dsc} = \frac{\Delta H_m}{\Delta H_m^0} \times 100\% \quad (1)$$

Where, $\chi_{c,dsc}$ (%) is the crystallinity of samples measured using DSC, ΔH_m (J/g) is the measured melting enthalpy from the DSC melting curve, $\Delta H_m{}^0$ (J/g) is the theoretical melting enthalpy of polyethylene with 100% crystallinity, with the value of $\Delta H_m{}^0$ = 288 J/g.[67,68]

4.3.5. Tensile Testing. Tensile tests were performed by using an Instron 5543A testing machine. Samples were prepared by hot pressing at 120 °C for 10 min, cooling to ambient temperature by removing the samples from the hot press, followed by cutting them into a dog-bone shape with the following dimensions: a gauge length of 20 mm, a width of 5 mm, and a thickness of 0.5 mm. *Note: The hot pressing was performed until defects in the samples disappeared.* Prior to testing, the specimens were conditioned at ambient temperature or placed in a desiccator for at least 24 h to ensure proper moisture equilibration. The tensile tests were conducted at room temperature with a cross-head speed of 5 mm/min.

4.3.6. Wide Angle X-Ray Scattering (WAXS). WAXS measurements were performed using a SAXSLab Ganesha system at the South Carolina SAXS Collaborative. The X-ray source was a Xenocs GeniX3D microfocus generator with a copper target, delivering a monochromatic X-ray beam with a wavelength of 0.154 nm. Two-dimensional scattering data were collected using a Pilatus 300K detector (Dectris), with pixel dimensions of 172 × 172 μm^2. The experiment was conducted with an X-ray flux of 36.3 million photons/s, and the sample-to-detector distance was set to 112.1 mm. Calibration of the system was performed using National Institute of Standards and Technology (NIST) reference material 640c (silicon). Data acquisition and reduction were carried out using SAXSGUI V2.23.23, with the 2D scattering patterns converted to 1D scattering curves. Polymer crystallinity (χ) was calculated from the WAXS patterns using eq 2:

$$\chi(\%) = [A_a(110) + A_a(200)/A_a(110) + A_a(200) + A_b] \times 100 \quad (2)$$

where A_a represents the integrated area of the Bragg peaks corresponding to the orthorhombic crystalline phase of polyethylene (PE), and A_b corresponds to the area of the

https://doi.org/10.1021/acs.macromol.5c00176
Macromolecules 2025, 58, 4070−4081

amorphous halo. A Voigt profile fit was used to extract the peak areas.

4.3.7. Filament Extrusion. The biobased polyester 3D-printing filament was extruded using an Xplore MC-5 microcompounder with a nozzle diameter of 1.75 mm. Prior to extrusion, the polymer was dried and melted under vacuum at 100 °C for 12 h in a vacuum oven. After drying, the polymer was cooled to room temperature under vacuum to form a thick film. This film was then manually cut into small pieces that were small enough to pass through the hopper of the extruder. Extrusion was carried out using a variable temperature profile, with the upper zone of the extruder set at 80 °C and the lower zone at 120 °C. The twin-screw motor speed was maintained at 200 rpm, with an applied torque of 500 N m. Typically, 4 g of polymer was extruded to fill the inner volume of the microcompounder. For consistent filament dimensions, continuous feeding of the polymer was required, and the filament was manually collected without the aid of a spooler. Using this method, more than 20 g of polymer were extruded in the form of a continuous piece of filament (PE-5,18). After the final loading of polymer, extrusion continued until the torque on the mixing screws remained stable for several minutes. Any remaining polymer was then mechanically recovered from the microcompounder.

4.3.8. 3D Printing. 3D printing of the polymer was completed via fused deposition modeling (FDM) on a Hyrel Hydra 21 printing platform. Filament feedstock for FDM was produced by using an extruder, where polymers were transformed into a molten state through a combination of shear and barrel heating. The material then passed through a filter screen and die, with extrusion performed at a die temperature of 120 °C and a screw speed of 30 rpm. Filaments were subsequently drawn onto winders with ample cooling to maintain a consistent diameter of 1.75 ± 0.05 mm. For FDM 3D printing, CAD models were generated and exported as stereolithography (STL) file types, and the Prusa software procedure was employed to convert the STL files into slices, align the model, and apply parameters for the 3D printer to utilize. For all prints, the layer thickness was set to 0.1 mm, with 100% infill and a printing speed of 15 mm/s for all movement operations.

■ ASSOCIATED CONTENT

Supporting Information

The Supporting Information is available free of charge at https://pubs.acs.org/doi/10.1021/acs.macromol.5c00176.

^{1}H NMR spectra and stacked HT-GPC traces of the corresponding polyesters and recycled PES-12,18; stacked FTIR, DSC, and WAXS of the polyesters; tensile tests of both low and high molecular weight polyesters; additional details of coarse-grained MD simulations of even-carbon-number polyesters; the melting temperature calculations as a function of the ester-to-methylene (E/M) ratio (PDF)

■ AUTHOR INFORMATION

Corresponding Authors

Chuanbing Tang − *Department of Chemistry and Biochemistry, University of South Carolina, Columbia, South Carolina 29208, United States;* orcid.org/0000-0002-0242-8241; Email: okuksen@clemson.edu

Olga Kuksenok − *Department of Materials Science and Engineering, Clemson University, Clemson, South Carolina 29634, United States;* orcid.org/0000-0002-1895-5206; Email: tang4@mailbox.sc.edu

Authors

Nagarjuna A. Mahadas − *Department of Chemistry and Biochemistry, University of South Carolina, Columbia, South Carolina 29208, United States*

Amir Suhail − *Department of Materials Science and Engineering, Clemson University, Clemson, South Carolina 29634, United States*

Martin Taylor Sobczak − *Department of Mechanical Engineering, College of Engineering, University of Georgia, Athens, Georgia 30602, United States;* orcid.org/0009-0002-0228-6658

Xiaomeng Li − *Department of Chemistry and Biochemistry, University of South Carolina, Columbia, South Carolina 29208, United States*

Kezhi Chen − *Department of Chemistry, University of Chicago, Chicago, Illinois 60637, United States*

Kenan Song − *Department of Mechanical Engineering, College of Engineering, University of Georgia, Athens, Georgia 30602, United States;* orcid.org/0000-0002-0447-2449

Guangbin Dong − *Department of Chemistry, University of Chicago, Chicago, Illinois 60637, United States*

Complete contact information is available at: https://pubs.acs.org/10.1021/acs.macromol.5c00176

Notes

The authors declare no competing financial interest.

■ ACKNOWLEDGMENTS

This work is supported by the U.S. National Science Foundation under the Center for Polymers for a Circular Economy (CHE-2317582). Many of the center's faculty and students participated in the discussion of this project. This project made use of the South Carolina SAXS Collaborative.

■ REFERENCES

(1) Geyer, R.; Jambeck, J. R.; Law, K. L. Production, use, and fate of all plastics ever made. *Sci. Adv.* **2017**, *3* (7), No. e1700782.

(2) Li, X.; Mahadas, N. A.; Zhang, M.; DePodesta, J.; Stefik, M.; Tang, C. Sustainable high-density polyethylene via chemical recycling: From modification to polymerization methods. *Polymer* **2024**, *295*, 126698.

(3) Sun, S.; Huang, W. Chemical upcycling of polyolefin plastics using structurally well-defined catalysts. *JACS Au* **2024**, *4*, 2081−2098.

(4) Strobl, G. R.; *The physics of polymers*; Springer, 1997; Vol. *2*.

(5) Meng, F.; Brandão, M.; Cullen, J. M. Replacing plastics with alternatives is worse for greenhouse gas emissions in most cases. *Environ. Sci. Technol.* **2024**, *58*, 2716−2727.

(6) Van Der Meulen, I.; Gubbels, E.; Huijser, S.; Sablong, R.; Koning, C. E.; Heise, A.; Duchateau, R. Catalytic ring-opening polymerization of renewable macrolactones to high molecular weight polyethylene-like polymers. *Macromolecules* **2011**, *44*, 4301−4305.

(7) Zeng, M.; Lee, Y.-H.; Strong, G.; LaPointe, A. M.; Kocen, A. L.; Qu, Z.; Coates, G. W.; Scott, S. L.; Abu-Omar, M. M. Chemical upcycling of polyethylene to value-added α,ω-divinyl-functionalized oligomers. *ACS Sustainable Chem. Eng.* **2021**, *9*, 13926−13936.

(8) Parke, S. M.; Lopez, J. C.; Cui, S.; LaPointe, A. M.; Coates, G. W. Polyethylene Incorporating Diels−Alder Comonomers: A "Trojan Horse" Strategy for Chemically Recyclable Polyolefins. *Angew. Chem., Int. Ed.* **2023**, *62*, No. e202301927.

(9) Arroyave, A.; Cui, S.; Lopez, J. C.; Kocen, A. L.; LaPointe, A. M.; Delferro, M.; Coates, G. W. Catalytic chemical recycling of post-consumer polyethylene. *J. Am. Chem. Soc.* **2022**, *144*, 23280−23285.
(10) Han, X.-W.; Zhang, X.; Zhou, Y.; Maimaitiming, A.; Sun, X.-L.; Gao, Y.; Li, P.; Zhu, B.; Chen, E. Y.-X.; Kuang, X.; et al. Circular olefin copolymers made de novo from ethylene and α-olefins. *Nat. Commun.* **2024**, *15* (1), 1462.
(11) Highmoore, J. F.; Kariyawasam, L. S.; Trenor, S. R.; Yang, Y. Design of depolymerizable polymers toward a circular economy. *Green Chem.* **2024**, *26*, 2384−2420.
(12) Aarsen, C. V.; Liguori, A.; Mattsson, R.; Sipponen, M. H.; Hakkarainen, M. Designed to Degrade: Tailoring Polyesters for Circularity. *Chem. Rev.* **2024**, *124*, 8473−8515.
(13) Arrington, A. S.; Brown, J. R.; Win, M. S.; Winey, K. I.; Long, T. E. Melt polycondensation of carboxytelechelic polyethylene for the design of degradable segmented copolyester polyolefins. *Polym. Chem.* **2022**, *13*, 3116−3125.
(14) Biermann, U.; Bornscheuer, U.; Meier, M. A.; Metzger, J. O.; Schäfer, H. J. Oils and fats as renewable raw materials in chemistry. *Angew. Chem., Int. Ed.* **2011**, *50*, 3854−3871.
(15) Jang, Y.-J.; Nguyen, S.; Hillmyer, M. A. Chemically Recyclable Linear and Branched Polyethylenes Synthesized from Stoichiometrically Self-Balanced Telechelic Polyethylenes. *J. Am. Chem. Soc.* **2024**, *146*, 4771−4782.
(16) Kocen, A. L.; Cui, S.; Lin, T.-W.; LaPointe, A. M.; Coates, G. W. Chemically recyclable ester-linked polypropylene. *J. Am. Chem. Soc.* **2022**, *144*, 12613−12618.
(17) Nomura, K.; Binti Awang, N. W. Synthesis of bio-based aliphatic polyesters from plant oils by efficient molecular catalysis: A selected survey from recent reports. *ACS Sustainable Chem. Eng.* **2021**, *9*, 5486−5505.
(18) Pepels, M. P.; Hansen, M. R.; Goossens, H.; Duchateau, R. From polyethylene to polyester: influence of ester groups on the physical properties. *Macromolecules* **2013**, *46*, 7668−7677.
(19) Zhao, Y.; Rettner, E. M.; Harry, K. L.; Hu, Z.; Miscall, J.; Rorrer, N. A.; Miyake, G. M. Chemically recyclable polyolefin-like multiblock polymers. *Science* **2023**, *382*, 310−314.
(20) Zhou, L.; Qin, P.; Wu, L.; Li, B.-G.; Dubois, P. Potentially biodegradable "short-long" type diol-diacid polyesters with superior crystallizability, tensile modulus, and water vapor barrier. *ACS Sustainable Chem. Eng.* **2021**, *9*, 17362−17370.
(21) Rist, M.; Greiner, A. Synthesis, Characterization, and the Potential for Closed Loop Recycling of Plant Oil-Based PA X. 19 Polyamides. *ACS Sustainable Chem. Eng.* **2022**, *10*, 16793−16802.
(22) Chikkali, S.; Stempfle, F.; Mecking, S. Long-Chain Polyacetals From Plant Oils. *Macromol. Rapid Commun.* **2012**, *33*, 1126−1129.
(23) Ortmann, P.; Heckler, I.; Mecking, S. Physical properties and hydrolytic degradability of polyethylene-like polyacetals and polycarbonates. *Green Chem.* **2014**, *16*, 1816−1827.
(24) Pemba, A. G.; Flores, J. A.; Miller, S. A. Acetal metathesis polymerization (AMP): A method for synthesizing biorenewable polyacetals. *Green Chem.* **2013**, *15*, 325−329.
(25) Roumanet, P.-J.; Jarroux, N.; Goujard, L.; Le Petit, J.; Raoul, Y.; Bennevault, V.; Guégan, P. Synthesis of linear polyesters from monomers based on 1, 18-(Z)-octadec-9-enedioic acid and their biodegradability. *ACS Sustainable Chem. Eng.* **2020**, *8*, 16853−16860.
(26) Zhou, C.; Wei, Z.; Yu, Y.; Shao, S.; Leng, X.; Wang, Y.; Li, Y. Biobased long-chain aliphatic polyesters of 1, 12-dodecanedioic acid with a variety of diols: Odd-even effect and mechanical properties. *Mater. Today Commun.* **2019**, *19*, 450−458.
(27) Eck, M.; Mecking, S. Closed-Loop Recyclable and Non-persistent Polyethylene-like Polyesters. *Acc. Chem. Res.* **2024**, *57*, 971−980.
(28) Quinzler, D.; Mecking, S. Linear semicrystalline polyesters from fatty acids by complete feedstock molecule utilization. *Angew. Chem., Int. Ed.* **2010**, *122*, 4402−4404.
(29) Häußler, M.; Eck, M.; Rothauer, D.; Mecking, S. Closed-loop recycling of polyethylene-like materials. *Nature* **2021**, *590*, 423−427.
(30) Birkle, M.; Mehringer, H. S.; Nelson, T. F.; Mecking, S. Aliphatic Polyester Materials from Renewable 2, 3-Butanediol. *ACS Sustainable Chem. Eng.* **2024**, *12*, 4156−4163.
(31) Huang, K.; Brentzel, Z. J.; Barnett, K. J.; Dumesic, J. A.; Huber, G. W.; Maravelias, C. T. Conversion of furfural to 1, 5-pentanediol: Process synthesis and analysis. *ACS Sustainable Chem. Eng.* **2017**, *5*, 4699−4706.
(32) Wijaya, H. W.; Kojima, T.; Hara, T.; Ichikuni, N.; Shimazu, S. Synthesis of 1, 5-Pentanediol by Hydrogenolysis of Furfuryl Alcohol over Ni−Y2O3 Composite Catalyst. *ChemCatchem* **2017**, *9*, 2869−2874.
(33) Eck, M.; Schwab, S. T.; Nelson, T. F.; Wurst, K.; Iberl, S.; Schleheck, D.; Link, C.; Battagliarin, G.; Mecking, S. Biodegradable High-Density Polyethylene-like Material. *Angew. Chem., Int. Ed.* **2023**, *135* (6), No. e202213438.
(34) Lu, J.; Wu, L.; Li, B.-G. High molecular weight polyesters derived from biobased 1, 5-pentanediol and a variety of aliphatic diacids: synthesis, characterization, and thermo-mechanical properties. *ACS Sustainable Chem. Eng.* **2017**, *5*, 6159−6166.
(35) Van Hoof, F. *Polyethylene terephthalate catalyzed by titanium (IV) butoxide*. Ph.D. Dissertation; UCL-Université Catholique de Louvain. 2012.
(36) Garcia, J. J.; Miller, S. A. Polyoxalates from biorenewable diols via Oxalate Metathesis Polymerization. *Polym. Chem.* **2014**, *5*, 955−961.
(37) Sahu, P.; Sharma, L.; Dawsey, T.; Gupta, R. K. Insight into the synthesis and thermomechanical properties of "short-long" type biobased aliphatic polyesters. *J. Appl. Polym. Sci.* **2024**, *141*, No. e54972.
(38) Ortmann, P.; Mecking, S. Long-spaced aliphatic polyesters. *Macromolecules* **2013**, *46*, 7213−7218.
(39) Witt, T.; Häußler, M.; Kulpa, S.; Mecking, S. Chain multiplication of fatty acids to precise telechelic polyethylene. *Angew. Chem., Int. Ed.* **2017**, *129*, 7697−7702.
(40) Li, X.; Suhail, A.; Mahadas, N. A.; Zhang, M.; Hu, Z.; Stefik, M.; Kuksenok, O.; Tang, C. Modulating Polyethylene Mimics with Degradability via Synthesis and Modeling. *Macromolecules* **2025**, *58*, 2094−2105.
(41) Russell, K.; Hunter, B.; Heyding, R. Monoclinic polyethylene revisited. *Polymer* **1997**, *38*, 1409−1414.
(42) Tsubakihara, S.; Yasuniwa, M. Melting and crystallization of ultra-high molecular weight polyethylene with appearance of hexagonal phase II. Strain-induced crystallization of thermal-contracted sample. *Polym. J.* **1996**, *28*, 563−567.
(43) Nunes, R. W.; Martin, J. R.; Johnson, J. F. Influence of molecular weight and molecular weight distribution on mechanical properties of polymers. *Polym. Eng. Sci.* **1982**, *22*, 205−228.
(44) Schirmeister, C. G.; Hees, T.; Licht, E. H.; Mülhaupt, R. 3D printing of high density polyethylene by fused filament fabrication. *Addit. Manuf.* **2019**, *28*, 152−159.
(45) Fischer, J. *Handbook of molded part shrinkage and warpage*; William Andrew, 2012.
(46) Arias, J. J. R.; Thielemans, W. Instantaneous hydrolysis of PET bottles: An efficient pathway for the chemical recycling of condensation polymers. *Green Chem.* **2021**, *23*, 9945−9956.
(47) Fall, W. S.; Baschnagel, J. R.; Lhost, O.; Meyer, H. Role of short chain branching in crystalline model polyethylenes. *Macromolecules* **2022**, *55*, 8438−8450.
(48) Meyer, H.; Müller-Plathe, F. Formation of chain-folded structures in supercooled polymer melts. *J. Chem. Phys.* **2001**, *115*, 7807−7810.
(49) Vettorel, T.; Meyer, H. Coarse graining of short polyethylene chains for studying polymer crystallization. *J. Chem. Theory Comput.* **2006**, *2*, 616−629.
(50) Fall, W. S.; Baschnagel, J. R.; Benzerara, O.; Lhost, O.; Meyer, H. Molecular simulations of controlled polymer crystallization in polyethylene. *ACS Macro Lett.* **2023**, *12*, 808−813.

https://doi.org/10.1021/acs.macromol.5c00176
Macromolecules 2025, 58, 4070−4081

(51) Luo, C.; Sommer, J.-U. Coding coarse grained polymer model for LAMMPS and its application to polymer crystallization. *Comput. Phys. Commun.* **2009**, *180*, 1382−1391.
(52) Luo, C.; Sommer, J.-U. Disentanglement of linear polymer chains toward unentangled crystals. *ACS Macro Lett.* **2013**, *2*, 31−34.
(53) Meyer, H.; Müller-Plathe, F. Formation of chain-folded structures in supercooled polymer melts examined by MD simulations. *Macromolecules* **2002**, *35*, 1241−1252.
(54) Sommer, J. U.; Luo, C. Molecular dynamics simulations of semicrystalline polymers: Crystallization, melting, and reorganization. *J. Polym. Sci., Part B: Polym. Phys.* **2010**, *48*, 2222−2232.
(55) Kuwata, M.; Zorn, S. R.; Martin, S. T. Using elemental ratios to predict the density of organic material composed of carbon, hydrogen, and oxygen. *Environ. Sci. Technol.* **2012**, *46*, 787−794.
(56) Marrink, S. J.; Risselada, H. J.; Yefimov, S.; Tieleman, D. P.; De Vries, A. H. The MARTINI force field: coarse grained model for biomolecular simulations. *J. Phys. Chem. B* **2007**, *111*, 7812−7824.
(57) Plimpton, S. Fast parallel algorithms for short-range molecular dynamics. *J. Comput. Phys.* **1995**, *117*, 1−19.
(58) Thompson, A. P.; Aktulga, H. M.; Berger, R.; Bolintineanu, D. S.; Brown, W. M.; Crozier, P. S.; In't Veld, P. J.; Kohlmeyer, A.; Moore, S. G.; Nguyen, T. D.; et al. LAMMPS-a flexible simulation tool for particle-based materials modeling at the atomic, meso, and continuum scales. *Comput. Phys. Commun.* **2022**, *271*, 108171.
(59) Humphrey, W.; Dalke, A.; Schulten, K. VMD: visual molecular dynamics. *J. Mol. Graphics* **1996**, *14*, 33−38.
(60) Groot, R. D.; Warren, P. B. Dissipative particle dynamics: Bridging the gap between atomistic and mesoscopic simulation. *J. Chem. Phys.* **1997**, *107*, 4423−4435.
(61) Jeong, C.; Starr, F. W.; Beers, K. L.; Douglas, J. F. Influence of functionalization on the crystallinity and basic thermodynamic properties of polyethylene. *Macromolecules* **2023**, *56*, 3873−3883.
(62) Hall, K. W.; Sirk, T. W.; Klein, M. L.; Shinoda, W. A coarse-grain model for entangled polyethylene melts and polyethylene crystallization. *J. Chem. Phys.* **2019**, *150* (24), 244901.
(63) Sliozberg, Y. R.; Yeh, I.-C.; Kröger, M.; Masser, K. A.; Lenhart, J. L.; Andzelm, J. W. Ordering and crystallization of entangled polyethylene melts under uniaxial tension: A molecular dynamics study. *Macromolecules* **2018**, *51*, 9635−9648.
(64) Yi, P.; Locker, C. R.; Rutledge, G. C. Molecular dynamics simulation of homogeneous crystal nucleation in polyethylene. *Macromolecules* **2013**, *46*, 4723−4733.
(65) Marxsen, S. F.; Häußler, M.; Eck, M.; Mecking, S.; Alamo, R. G. Effect of CH2 run length on the crystallization kinetics of sustainable long-spaced aliphatic polyesters. *Polymer* **2023**, *282*, 126181.
(66) Ren, Y.; Sun, X.; Chen, L.; Li, Y.; Sun, M.; Duan, X.; Liang, W. Structures and impact strength variation of chemically crosslinked high-density polyethylene: effect of crosslinking density. *RSC Adv.* **2021**, *11*, 6791−6797.
(67) Cui, W.; Bian, Y.; Zeng, H.; Zhang, X.; Zhang, Y.; Weng, X.; Xin, S.; Jin, Z. Structural and tribological characteristics of ultra-low-wear polyethylene as artificial joint materials. *J. Mech. Behav. Biomed. Mater.* **2020**, *104*, 103629.
(68) Mirabella, F. M.; Bafna, A. Determination of the crystallinity of polyethylene/α-olefin copolymers by thermal analysis: Relationship of the heat of fusion of 100% polyethylene crystal and the density. *J. Polym. Sci., Part B: polym. Phys.* **2002**, *40*, 1637−1643.

https://doi.org/10.1021/acs.macromol.5c00176
Macromolecules 2025, 58, 4070−4081